

High-spin states of $J^\pi = 12^-, 14^-$ in ^{208}Pb studied by (e, e')

J. Lichtenstadt, J. Heisenberg,* C. N. Papanicolas, and C. P. Sargent

Bates Linear Accelerator Center and Massachusetts Institute of Technology, Cambridge, Massachusetts 02139

A. N. Courtemanche and J. S. McCarthy

University of Virginia, Charlottesville, Virginia 22901

(Received 2 March 1979)

Inelastic electron scattering cross sections for the excited states at 6.43, 6.74, and 7.06 MeV in ^{208}Pb were measured with high resolution. The measurements were done in forward and backward directions covering the momentum transfer range of $0.3 < q < 2.5 \text{ fm}^{-1}$. The state at 7.06 MeV was identified as the $\pi(i_{13/2}h_{11/2}^{-1})_{12^-}$ and the states at 6.74 and 6.43 MeV as the $\nu(j_{15/2}i_{13/2}^{-1})_{14^-, 12^-}$, respectively. The identification was based on four criteria: (a) the agreement between the q dependence of the measured form factor with that of Hartree-Fock single particle-hole prediction, with no adjustment of radial parameters, (b) the absence of a longitudinal form factor, (c) the relative magnitude of the observed levels, and (d) the excitation energies being close to the single p-h energies. The measured strength of each state was found to be 50% of the single p-h prediction.

NUCLEAR REACTIONS $^{208}\text{Pb}(e, e')E=50\text{--}335 \text{ MeV}$; measured $\sigma(E)$, $\theta=90^\circ, 160^\circ$. ^{208}Pb deduced, levels $J^\pi=12^-, 14^-$. DWBA calculation with Hartree-Fock single particle wave functions.

I. INTRODUCTION

The ^{208}Pb nucleus has been subject of several (e, e') experiments.¹⁻⁴ The existing high energy data have been limited by the lack of resolution to only those of strong and well separated states, while at low energy they have been limited to low-spin states where the levels could be identified and interpreted without high momentum transfer data. The Bates accelerator electron scattering facility with its high resolution, high incident beam currents and moderately high incident energies, now makes possible the detection of relatively weak states in regions where the density of levels is high.

The ^{208}Pb nucleus has closed neutron and proton shells. The dominant excitations at low energy and momentum transfer are the well known collective excitations of relatively low spin. These are interpreted as a large number of single particle-hole (p-h) excitations coupled together to the collective state of spin and parity J^π . On the other hand, the number of single particle-hole transitions which can couple to large J is usually considerably smaller, thus collectivity is less likely to build up. Such high-spin states then can have a very pure composition, and their investigation through electron scattering or other probes is particularly interesting.

The particle-hole components at p-h energies below 8 MeV which give rise to states with spins above 9 are listed in Table I. Among these is only one p-h transition which couples to $J^\pi = 14^-$, and

only two which couple to $J^\pi = 12^-$. States dominated by such single p-h transitions cannot be called collective. However, because of the high occupation number of the levels involved, many nucleons participate in these transitions resulting in substantial cross sections. For some of the listed p-h transitions the cross sections, calculated in Born approximation using Hartree-Fock wave functions, are shown in Fig. 1.

With all the multitude of shapes of form factors to be expected, electron scattering can contribute the following criteria for the identification of states: (a) The exact matching of the q dependence of the form factor. (b) For the identification of magnetic excitations, the absence of a longitudinal form factor is a necessary condition (but not sufficient). (c) The relative magnitude of all the observed levels. (d) The observed excitation energies that are close to the p-h energies. When all four criteria are considered for certain cases, they alone can make a very convincing identification. The identification and interpretation of the natural parity (electric) states is still underway, as more p-h transitions exist that can mix. Preliminary results identifying the magnetic high-spin states, namely, the $\pi(i_{13/2}, h_{11/2}^{-1})_{12^-}$ and the $\nu(j_{15/2}, i_{13/2}^{-1})_{14^-, 12^-}$, have been published.⁵ We shall present in this paper new backward angle measurements, as well as the measurements of the form factor for the 14^- state at 6.74 MeV, confirming those results.

The full experiment included a comparison of the different lead isotopes, which will be pre-

TABLE I. High-spin ($J > 9$), single p-h transitions in ^{208}Pb , whose single p-h energies are below 8 MeV.

Transition	$E_{\text{sp}} \text{ (MeV)}$	Magnetic		Electric		
Neutron (p-h)						
$2g_{9/2} \ i_{13/2}$	5.06		11^+	9^+		10^+
$j_{15/2} \ 2f_{5/2}$	5.42			9^+		10^+
$j_{15/2} \ 3p_{3/2}$	5.66			9^+		
$i_{11/2} \ i_{13/2}$	5.84		11^+	9^+	12^+	10^+
$j_{15/2} \ i_{13/2}$	6.48	14^-	12^-	10^-	13^-	11^-
$i_{11/2} \ 2f_{7/2}$	6.55					9^-
$3d_{5/2} \ i_{13/2}$	6.63			9^+		
$2g_{9/2} \ h_{9/2}$	6.84					9^-
$j_{15/2} \ 2f_{7/2}$	7.19		11^+	9^+		10^+
$2g_{7/2} \ i_{13/2}$	7.55			9^+		10^+
$i_{11/2} \ h_{9/2}$	7.62			10^-		9^-
Proton (p-h)						
$h_{9/2} \ h_{11/2}$	5.65			9^+		10^+
$2f_{7/2} \ h_{11/2}$	6.54			9^+		
$i_{13/2} \ h_{11/2}$	7.26	12^-	10^-		11^-	9^-
$i_{13/2} \ 2d_{5/2}$	7.59			9^+		

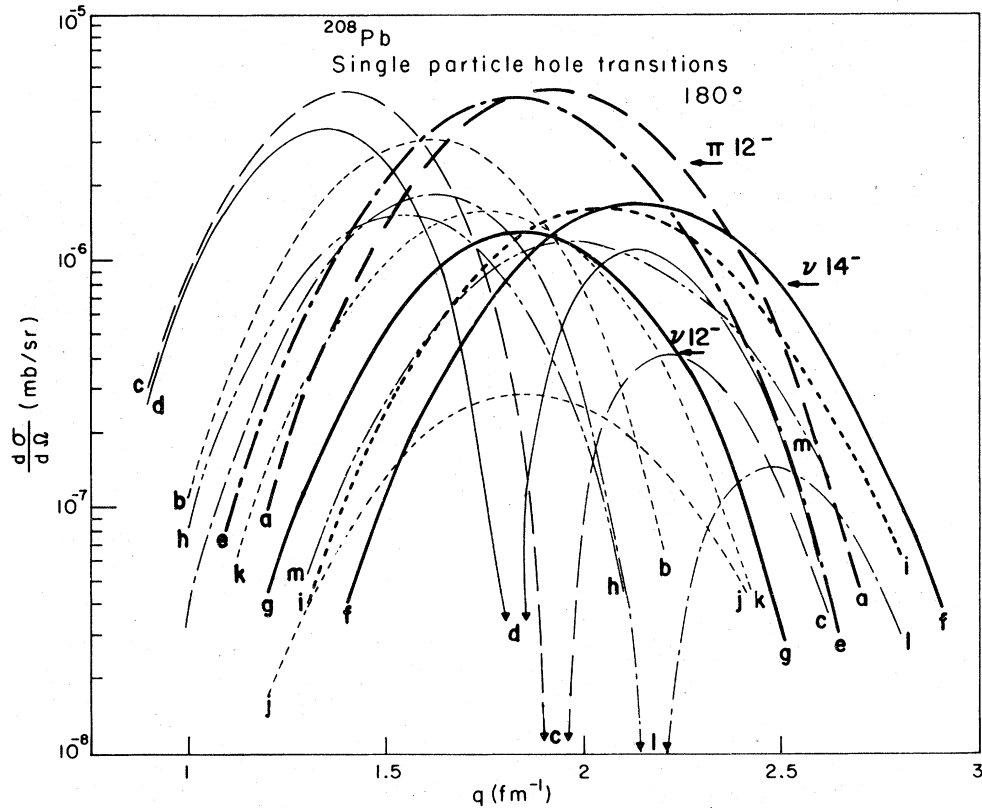


FIG. 1. Cross sections of high-spin, single particle hole transitions in ^{208}Pb calculated in Born approximation. Shown are the following transitions: Proton: a, b ($i_{13/2}h_{11/2}^{-1}$) $_{12^-,10^-}$, c ($i_{13/2}2d_{5/2}^{-1}$) $_{9^+}$, d ($2f_{7/2}h_{11/2}^{-1}$) $_{9^+}$, e ($h_{9/2}, h_{11/2}^{-1}$) $_{10^+}$. Neutron: f-h ($j_{15/2}i_{13/2}^{-1}$) $_{14^-,12^-,10^-}$, i-k ($i_{11/2}i_{13/2}^{-1}$) $_{12^+,11^+,10^+}$, l ($j_{15/2}2f_{7/2}^{-1}$) $_{11^+}$, m ($i_{11/2}h_{9/2}^{-1}$) $_{10^-}$.

sented, together with the full experimental details in a forthcoming paper.⁶ Here we shall describe only briefly the experimental details (Sec. II). Section III contains the results, followed by comments on the distorted-wave Born approximation (DWBA) analysis and a discussion in Secs. IV and V.

II. EXPERIMENTAL METHOD AND DATA REDUCTION

The experiments were done using incident energies between 50 and 335 MeV, detecting the scattered electrons at 90° and 160° . The momentum transfer region covered was $0.3 < q < 2.5 \text{ fm}^{-1}$ at 90° and $0.8 < q < 2.5 \text{ fm}^{-1}$ at 160° . The inelastic electron scattering cross section is given in Born approximation by

$$\frac{d\sigma}{d\Omega} = \frac{d\sigma}{d\Omega}_{\text{Mott}} \left\{ |F_L^C(q)|^2 + \left[\frac{1}{2} + \tan^2\left(\frac{1}{2}\theta\right) \right] \times \left[|F_T^C(q)|^2 + |F_T^M(q)|^2 \right] \right\}, \quad q = 2E \sin\frac{1}{2}\theta. \quad (1)$$

The extra factor of $(\frac{1}{2} + \tan^2\frac{1}{2}\theta)$ in front of the sum over the transverse form factors allows a separation of the longitudinal form factor F_L^C , from the transverse form factors F_T^C and F_T^M , using the total cross section measured in different directions (90° and 160°) in Born approximation. This separability is not restricted to Born approximation. For example, the curves to be shown in Figs. 3 and 4 were calculated in DWBA at both 90° and 160° . The resulting cross sections when divided by $\sigma_M [\frac{1}{2} + \tan^2(\frac{1}{2}\theta)]$ and plotted versus $q_{\text{eff}} = q(1 + 4Z\alpha/3EA^{1/3})$, to correct for the distortion of the electron waves, are almost identical.

The targets used were ^{208}Pb foils 99.9% enriched, of 30 and 10 mg/cm² thickness. The 30 mg/cm² target was used in transmission mode for the 90° measurements, while the 10 mg/cm² was used in the 160° measurements in reflection mode. Special cooling arrangements allowed beam currents up to 45 μA .

The scattered electrons were analyzed with the high resolution energy loss spectrometer.⁷ A solid angle of 3.1 msr was utilized. The momentum acceptance was limited to 5% to avoid inefficiencies near the edges of the detector.

The incident electron energies as well as the spectrometers linear and quadratic dispersion parameters were obtained by measuring the recoil energy differences between elastic peaks of ^9Be , ^{16}O , ^{27}Al , and ^{208}Pb , together with the peak locations of excited states with well known excitation energies in these nuclei. The magnetic field in the spectrometer was measured with a NMR probe. The resulting uncertainty in the incident beam energy was typically 0.2%.

The 90° data were normalized to the elastic

^{208}Pb cross section, calculated with a phase shift code, from the best fit to all available (e, e') and muonic x-ray transitions data.⁸ At 160° we took absolute measurements, since the elastic peak was too weak to determine a normalization. Comparison of the measured cross sections, when possible (energies below 180 MeV), with the calculated ones gave agreement within $\pm 5\%$. A total of 17 spectra have been taken at 90° , and 14 spectra at 160° .

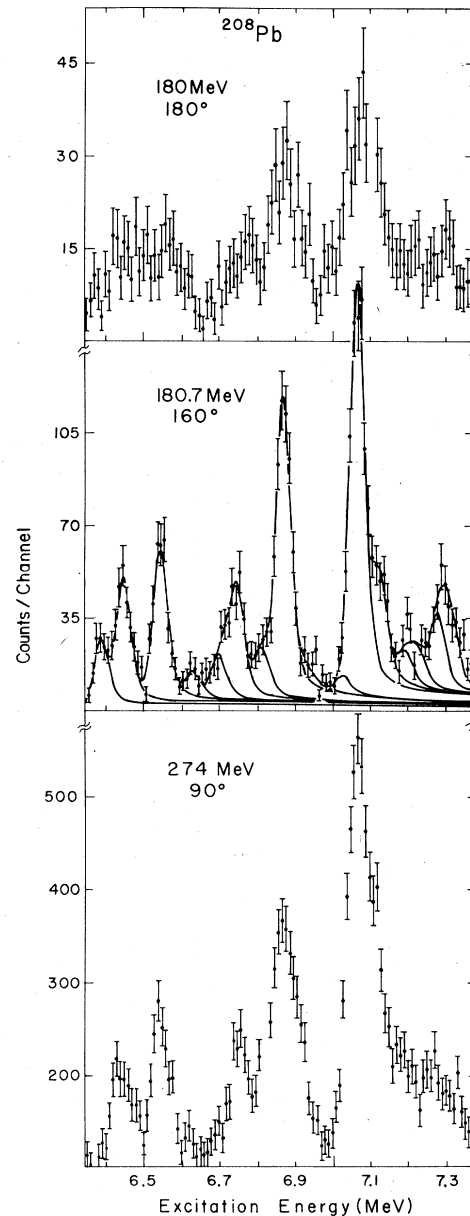


FIG. 2. (e, e') spectra from ^{208}Pb taken at forward and backward directions. The spectrum at 180° was taken by Lindgren *et al.* (Ref. 12).

To extract the cross sections, a line shape fitting code was used, in which an asymmetric Gaussian shape is folded with the effects of Landau straggling, bremsstrahlung, and emission of Schwinger radiation using the method of Bergstrom.⁹ In the fitting process more than 40 levels have been fitted to each spectrum. In general the peak shape was "locked" to the shapes of strong peaks which were known to be well separated. The excitation energies of the fitted levels were allowed to vary only when the peaks were well defined. Otherwise the excitation energies were locked too, to the known energy of a close strong peak. As a guide we used the excitation energies obtained by the (p, p') experiment by Wagner *et al.*¹⁰

III. RESULTS

Typical spectra taken at 90° and 160° are shown in Fig. 2, together with a ²⁰⁸Pb spectrum taken at 180° by Lindgren *et al.*¹¹ A best fit to the 160° data is also shown. A comparison of the 90° and 160° spectra shows that above 6 MeV of excitation, most of the states have a substantial transverse form factor. It should be noted that the data taken at 180° look very similar to the data taken at 160°. This is due to the transverse nature of most of the observed cross section in this excitation region. Measurements at 180° would then gain very little in comparison to measurements at 160°, while increasing the complexity of the ex-

perimental setup.

The incident energies in the experiment and the extracted cross sections of the states at 6.43, 6.75, and 7.06 MeV, which will be identified as the 12⁻, 14⁻, 12⁻ states, respectively, are given in Table II. The uncertainty in the excitation energies of these states is 15 keV for the 6.43 MeV state and 10 keV for the other two. The cross sections given are already corrected for finite acceptance of the spectrometer, for multiple scattering, and for the energy spread in the incident beam. The errors in the cross sections given in Table II are the statistical errors. There is an additional 5% uncertainty coming from the target thickness and the absolute normalization, not included in the table. This is a correlated uncertainty which does not affect the q dependence, but is an uncertainty in the overall observed strength.

According to Eq. (1), at 90° where $[\frac{1}{2} + \tan^2(\frac{1}{2}\theta)] = 1.5$, the longitudinal and the transverse form factors contribute to the cross section according to their magnitude with about the same weight. At 160° the contribution from the transverse cross section is enhanced by a factor of 32. To demonstrate its transverse nature, we plotted the cross section divided by $\sigma_M [\frac{1}{2} + \tan^2(\frac{1}{2}\theta)]$ vs q_{eff} , thus assuming a purely transverse form factor. The q_{eff} , which was used only for plotting purposes, corrects approximately for the distortion effects on the electron wave. These plots are shown in Figs. 3 and 4.

TABLE II. Experimental cross sections measured for the excited states at 6.43, 6.74, and 7.06 MeV. Errors are the statistical errors only. The number following E is the power of 10 which multiplies the preceding number ($En \equiv 10^n$).

E (MeV)	%	6.43 MeV (mb/sr)	%	6.74 MeV (mb/sr)	%	7.06 MeV (mb/sr)	%
90°							
201.53	0.22					2.15E-6	15.5
213.85	0.21	5.44E-7	97			3.59E-6	22
236.85	0.15	1.60E-6	13.5	4.06E-7	54	2.58E-6	11
255.96	0.13	1.39E-6	12.5	1.26E-6	13.5	3.72E-6	7.1
273.97	0.18	9.64E-7	7.3	1.01E-6	7.6	3.46E-6	3.4
298.59	0.17	4.36E-7	14	1.30E-6	5.6	1.93E-6	5.9
335.40	0.22	2.03E-7	30	1.04E-6	12	6.96E-7	12
160°							
140.69	0.11	2.56E-7	40	1.16E-7	74	8.23E-7	20
149.97	0.22	3.30E-7	21	1.84E-7	28	1.70E-6	8.9
165.29	0.12	6.61E-7	12	3.35E-7	23	2.36E-6	5.8
180.70	0.25	8.71E-7	8.2	7.90E-7	9.0	2.89E-6	4.3
195.27	0.26	5.74E-7	9.4	7.85E-7	7.6	2.43E-6	4.0
210.99	0.10	3.39E-7	13.5	9.91E-7	6.9	1.37E-6	6.0
225.12	0.17	1.53E-7	22	9.20E-7	6.8	9.64E-7	6.6
240.07	0.22	6.70E-8	24	5.33E-7	7.5	2.17E-7	14.5
255.12	0.22	1.42E-8	59	9.34E-8	19	5.09E-8	27

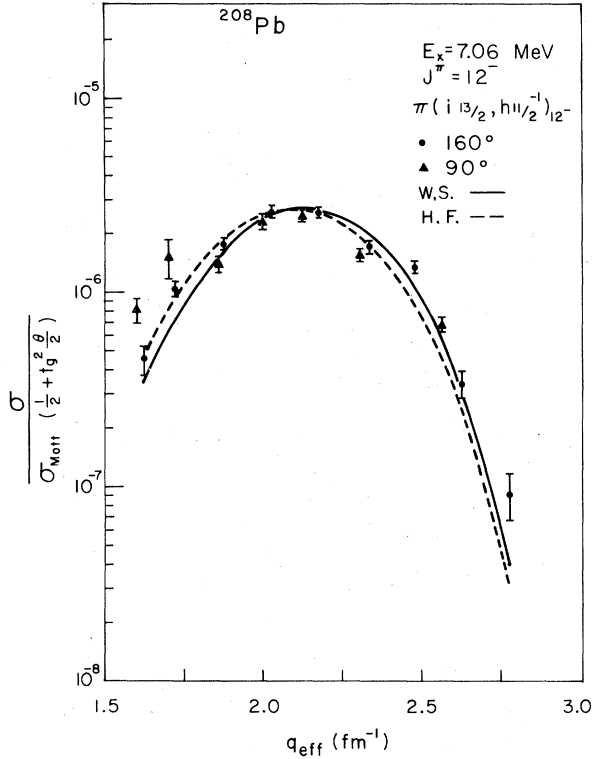


FIG. 3. Cross section of the level at 7.06 MeV with $J^\pi = 12^-$. The dashed and solid lines are single p-h predictions of the $\pi(i_{13/2}, h_{11/2}^{-1})_{12^-}$ transition, using Hartree-Fock and Woods-Saxon wave functions, respectively. The curves presented are the "reduced cross sections" calculated in DWBA at 160° . The calculation at 90° is almost identical to that at 160° , to the accuracy of the graph.

IV. DWBA ANALYSIS

In the Born approximation the form factor of the magnetic transition $M\lambda$ is calculated from the current density $\rho_{\lambda\lambda}$ by

$$\rho_{\lambda\lambda}^M = \frac{\hbar}{2Mc} \sum_{ph} i^{l_p - l_h + 1} (-1)^{\lambda + j_h + 1/2} \mu_s \begin{pmatrix} j_p & j_h & \lambda \\ \frac{1}{2} & -\frac{1}{2} & 0 \end{pmatrix} \frac{\hat{j}_p \hat{j}_h}{[4\pi\lambda(\lambda+1)]^{1/2}} \left[\frac{\lambda(\lambda+1)}{r} + (x_p + x_h) \left(\frac{d}{dr} + \frac{1}{r} \right) \right] U_p^*(r) U_h(r), \quad (3)$$

$$x_p = (l_p - j_p)(2j_p + 1), \quad \mu_s^{\text{proton}} = 2.79\mu_N, \quad \mu_s^{\text{neutron}} = 1.91\mu_N,$$

where μ_N is the nuclear magneton, and M the nucleon mass. This is then folded with the proton size. Simplifying the expression given by Lee, the contribution from the convection current is given by

$$\rho_{\lambda\lambda}^C = \frac{(-1)^{j_h - 1/2}}{\lambda(4\pi)^{1/2}} \hat{j}_p \hat{j}_h \hat{l}_p \hat{l}_h \begin{Bmatrix} l_p & l_h & \lambda \\ j_p & j_h & \frac{1}{2} \end{Bmatrix} \{ [l_h(l_h+1)]^{1/2} \langle l_p 0 l_h 1 | \lambda 1 \rangle + [l_p(l_p+1)]^{1/2} \langle l_h 0 l_p 1 | \lambda 1 \rangle \} \frac{U_p^*(r) U_h(r)}{r}. \quad (4)$$

This contribution is folded with the charge distribution of the proton or the neutron. All the calculations were done in DWBA using the above current distributions with the computer code

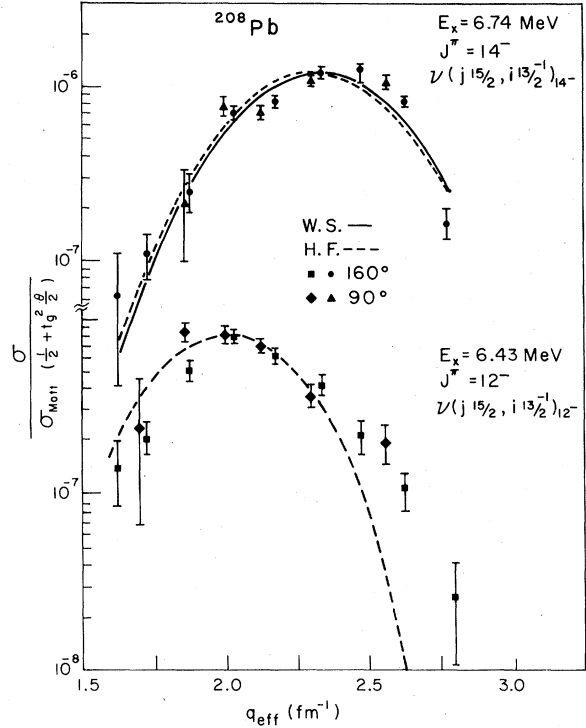


FIG. 4. Cross sections of the levels at 6.74 and 6.43 MeV, with $J^\pi = 14^-, 12^-$, respectively. The dashed and solid lines are single p-h predictions of the $\nu(j_{15/2}, i_{13/2}^{-1})_{14^-, 12^-}$ transitions, using Hartree-Fock and Woods-Saxon wave functions, respectively. For calculational details see text.

$$F^M(q^2) = \frac{(4\pi)^{1/2}}{Z} \frac{\hat{J}_f}{\hat{J}_i} \int \rho_{\lambda\lambda}(r) j_\lambda(q \cdot r) r^2 dr, \quad (2)$$

$$\hat{j} = (2j+1)^{1/2}, \quad \rho_{\lambda\lambda} = \rho_{\lambda\lambda}^C + \rho_{\lambda\lambda}^M.$$

The total current density has contributions from the magnetization current and from the convection current. Following Lee,¹² the magnetization current is determined from the radial shapes of the particle and the hole wave functions, $U_p(r)$ and $U_h(r)$, by

HEIMAG.¹³

To test the code we calculated the cross section setting the nuclear charge to $Z=1$, thus turning off the distortion of the electron waves, and there-

by reproducing essentially the Born approximation result. The latter in turn was compared to the result obtained from the code MICRODENS,¹² using harmonic oscillator wave functions.

V. DISCUSSION

The identification of the states was done following the four criteria mentioned in the Introduction. These are the q dependence of the form factor, the absence of a longitudinal form factor, the relative strength of the levels, and the closeness of their excitation energies to the single p-h energies.

The excellent agreement between the reduced cross sections ($\sigma/\sigma_{\text{Mott}} [\frac{1}{2} + \tan^2(\frac{1}{2}\theta)]$) taken at 90° and at 160° indicates that our results are consistent with the assumption of purely transverse form factors. The 90° data agree also very well with the fit which will be discussed later. The fit is essentially determined by the 160° data, and shows that any longitudinal form factor must be less than $\sim 10\%$ of the transverse form factor.

Of the three states the stronger one is observed at 7.06 MeV of excitation, and the other two are close in their excitation energies, which are 6.43 and 6.74 MeV. We identify the state at 7.06 MeV as the $\pi(i_{13/2}h_{11/2}^{-1})_{12^-}$ transition whose single p-h energy is 7.20 MeV, and the states at 6.74 and 6.43 MeV as the $\nu(j_{15/2}i_{13/2}^{-1})_{14^-,12^-}$, with single p-h energy of 6.48 MeV. The observed excitation energies are very close to the single p-h energies and the observed relative strengths follow the predicted ones as can be seen in Fig. 1.

In the identification process we compared the measured cross sections to the calculated ones of the single p-h transitions. We chose the wave functions generated from the self-consistent Hartree-Fock (HF) potential using the DME interaction of Negele and Vautherin.¹⁴ These single particle wave functions reproduce the elastic scattering from ^{208}Pb up to the third maximum, as well as predict the proper q dependence of the Coulomb form factor for the 10^+ state at 4.89 MeV (Ref. 5) over the first maximum.

The choice of HF wave functions to identify the transitions is of significance, since it avoids an adjustable radial parameter to be fitted. As can be seen from Fig. 1, form factors of different multipolarities do not necessarily differ strongly from each other in the location of their first maximum. Using harmonic oscillator wave functions, or Woods-Saxon wave functions, where the well size parameter is adjustable could lead to incorrect interpretation, as a change in this parameter would shift the form factor in q space.

The calculated form factors were fitted to the data for each level by varying only the overall

strength. These fits are presented by the solid lines in Figs. 3 and 4 together with the experimental results. The agreement between the calculation and the experiment, as seen from these figures, is excellent.

After the positive identification was made using the HF wave functions, we repeated the calculations using Woods-Saxon wave functions, fitting the well size parameter as well as the overall strength. In these calculations we fitted the neutron well size to the 14^- data, and the proton well size to the 12^- state at 7.06 MeV. The well radius came out to be 1.255 ± 0.003 fm for both configurations. The cross sections, which are almost identical to those obtained from the HF prediction are shown in Figs. 3 and 4 as well.

Finally we tried other single p-h interpretations. These gave much worse χ^2 in the fit, even when configurations which should be *a priori* excluded, since their p-h energies are too far away from the observed energies, were considered. The form factor of the state at 6.43 MeV for example, has a shape close to that of the $(i_{11/2}h_{9/2}^{-1})_{10^-}$ transition. This, however, has a single p-h energy above 7.6 MeV, and as such is a very unlikely interpretation.

It should be noted that the density of states in this region of excitation energy is very high. This high density consists mainly of lower-spin states, where many single p-h transitions can contribute, and fractionation may occur, as observed in the $M1$ states.¹⁵ It must be considered then that within our resolution several states can contribute to the total observed cross section. There are, however, a few considerations which experimentally help. The lower-spin states have their first maximum of the form factor usually at lower momentum transfer. Thus the observed form factors in these excitation energies at low momentum transfer can be used to estimate the background contributions from such low-spin states to the form factor of the adjacent high-spin state. The background for the three states discussed here was estimated to be smaller than the statistical uncertainties. On the other hand, the density of the high-spin states is low, which makes it very unlikely that the observed form factors stem from two or more unresolved high-spin states. Also such a mixture generally would not agree with a q dependence of a single configuration.

The overall strength observed when fitted either with HF wave functions or with the Woods-Saxon wave functions comes out to be only $(50 \pm 3.5)\%$ of the predicted single particle strength for the $\nu(j_{15/2}, i_{13/2})_{14^-,12^-}$, as well as for the $\pi(i_{13/2}, h_{11/2}^{-1})_{12^-}$ configuration. This quenching is about the same as that observed in the $M9$ moment of the ground state of ^{209}Bi , coming from the odd $h_{9/2}$ proton.¹⁶

Several effects might cause this quenching: In our calculations, no exchange currents have been included, nor have we included any many-particle-many-hole configurations in the wave functions. We have also ignored any "core polarization" due to the spin exchange part of the interaction. While exchange currents seem to increase the cross section,¹⁷ the many-particle-many-hole configurations reduce the overall strength. The core polarization similarly to the induced or effective charge leads to an additional magnetization, and because of the repulsive nature of the interaction tends to reduce the total magnetization observed. These effects have been parameterized by Ring and Speth¹⁸ introducing an effective magnetic operator $g_{\text{eff}} = 0.89 \times g_{\text{free}}$. Generally one would expect that the effects of exchange currents as well as the "core polarization" will introduce some additional q dependence as observed in (e, e') charge scattering.¹⁹ However, we observe in this experiment only the first maximum of the form factors, thus the sensitivity of these data to an additional q dependence is rather limited. Also one would expect that as these effects are "located" mostly at the nuclear surface, the form factors of the corrections will be similar to the observed form factors.

VI. SUMMARY

The (e, e') cross sections of the excited states at 6.43, 6.74, and 7.06 MeV have been measured

in forward and backward directions. The data indicate that these cross sections are purely transverse. The multipolarities of these states have been shown to be 12^- , 14^- , and 12^- , resulting from the single p-h transitions $\nu(j_{15/2}, i_{13/2}^{-1})_{12^-, 14^-}$ and $\pi(i_{13/2}, h_{11/2}^{-1})_{12^-}$, respectively. The identification was based on the agreement of the q dependence of the cross sections with the predictions of Hartree-Fock wave functions, the relative strengths, and the excitation energies of these states. The overall strength observed is 50% of the single particle prediction.

Further investigation of all the levels observed in this experiment is underway in order to identify other expected high spin states.

ACKNOWLEDGMENTS

The authors wish to thank P. Demos and W. Bertozzi for their continuous support in all phases of the experiment, W. Turchinets, S. Kowalski, C. F. Williamson, and P. C. Dunn for their expert advice during the performance of the experiment, D. Day and R. Altemus for their help in data taking, and J. Speth for the discussions about the interpretation of the results. We would like to thank R. A. Lindgren and G. Peterson for making available the 180° data for this publication. This work was supported by U. S. D. O. E. Contract No. EY-76-C-02-3069.

*Present address: University of New Hampshire, Durham, N. H. 03824.

¹J. Freidrich, Nucl. Phys. **A191**, 118 (1972).

²H. Rothaas, J. Friedrich, K. Merle, and B. Dreher, Phys. Lett. **51B**, 23 (1974).

³J. Friedrich, N. Voegler, and H. Euteneuer, Phys. Lett. **64B**, 269 (1976).

⁴R. Frey, A. Richter, A. Schwierczinski, E. Spamer, O. Titze, and W. Knupfer, Phys. Lett. **74B**, 45 (1978).

⁵J. Lichtenstadt, J. Heisenberg, C. N. Papanicolas, C. P. Sargent, J. S. McCarthy, and A. N. Courtemanche, Phys. Rev. Lett. **40**, 1127 (1978).

⁶C. N. Papanicolas, J. Heisenberg, J. Lichtenstadt, and J. S. McCarthy, (unpublished).

⁷W. Bertozzi *et al.*, Nucl. Instrum. Methods **141**, 457 (1977).

⁸J. L. Friar, J. Heisenberg, and J. W. Negele, in *Proceedings of the June Workshop in Intermediate Energy Electromagnetic Interactions with Nuclei*, edited by A. M. Bernstein (Massachusetts Institute of Technology, Cambridge, Massachusetts, 1977), p. 325.

⁹J. Bergstrom, in *Medium Energy Nuclear Physics*, M.I.T. 1967 Summer Study, edited by W. Bertozzi and S. Kowalski (Massachusetts Institute of Technology,

Cambridge, Massachusetts, 1967), p. 251.

¹⁰W. T. Wagner, G. M. Crawley, G. R. Hammerstein, and H. McManus Phys. Rev. C **12**, 757 (1975).

¹¹R. A. Lindgren *et al.*, private communication.

¹²H. C. Lee, Nuclear Charge, Convection Current and Magnetization Current Densities, AECL 4839 Chalk River, Ontario, 1975 (unpublished).

¹³J. Heisenberg, code HEIMAG (unpublished).

¹⁴J. W. Negele and D. Vautherin, Phys. Rev. C **5**, 1472 (1972).

¹⁵T. -S. H. Lee and S. Pittel, Phys. Rev. C **11**, 607 (1975); J. S. Dehesa, J. Speth, and A. Faessler, Phys. Rev. Lett. **38**, 208 (1977).

¹⁶P. K. A. de Witt Huberts, in *Proceedings of the Conference 'Modern Trends in Elastic Electron Scattering'*, edited by C. de Vries (Instituut voor Kernfysisch Onderzoek, Amsterdam, the Netherlands, 1978), p. 21.

¹⁷A. Arima, Y. Horikawa, H. Hyuga, and T. Suzuki, Phys. Rev. Lett. **40**, 1001 (1978).

¹⁸P. Ring and J. Speth, Nucl. Phys. **A235**, 315 (1974).

¹⁹C. N. Papanicolas, J. Heisenberg, J. Lichtenstadt, J. S. McCarthy, and A. N. Courtemanche, Phys. Rev. Lett. **41**, 537 (1978).